Arabian Journal for Science and Engineering (2024) 49:3267–3284
https://doi.org/10.1007/s13369-023-07973-9

RESEARCH ARTICLE-COMPUTER ENGINEERING AND COMPUTER SCIENCE

A Hybrid Deep Learning Framework to Predict Alzheimer's Disease Progression Using Generative Adversarial Networks and Deep Convolutional Neural Networks

Rajarshi SinhaRoy[1] · **Anupam Sen**[2]

Received: 25 September 2022 / Accepted: 23 May 2023 / Published online: 9 June 2023

Abstract

A major research subject in recent times is Alzheimer's disease (AD) due to the growth and considerable societal impacts on health. So, the detection of AD is essential for medication care. Early detection of AD is critical for effective treatment, and monitoring the time period between normal aging's unavoidable cognitive loss and dementia's more catastrophic degradation is common practice. The deep learning method for early diagnosis and automated categorization of AD has suddenly gained a lot of attention since rapid advancement in the field of GANs approaches has now been used in the clinical research sector. Many recent studies using brain MRI images and convolutional neural networks (CNNs) to identify Alzheimer's disease have yielded promising results. Instead of adequately engaging with the lack of real data, many research papers have focused on prediction. The main purpose of this paper is to do this by generating synthetic MRI images using a series of DCGANs. This paper demonstrates the effectiveness of this concept by cascading DCGANs that imitate different stages of Alzheimer's disease and utilizing SRGANs to enhance the resolution of MRI scans. The purpose of this research is to come forward and tell if an individual might just get Alzheimer's disease. CNN, DCGANs, and SRGANs are used in this paper to present a deep learning-based approach that improves classification and prediction accuracy to 99.7% and also handles the lack of data and the resolution of data.

Keywords Alzheimer's disease · Convolutional neural networks · Deep convolutional GANs · Super-resolution GANs · Healthcare · Generative adversarial networks

1 Introduction

Alzheimer's disease is a degenerative neural disorder that affects memory and cognitive abilities. Early diagnosis and medication during the initial stages of Alzheimer's disease have the highest possibility of slowing or stopping the disease. Alzheimer's-related brain alterations can start three to ten years before symptoms occur, and in extreme cases, more than 30 years. Magnetic resonance imaging (MRI) is a noninvasive testing tool that can detect structural alterations in the brain early on. This human disease's initial stages include recalling recent incidents or discussions. The degrees of the disorder are as follows: Mild, moderate, and severe are the three levels of severity. Alzheimer's disease as well as other kinds of dementia affects well over 4 million individuals in India. The deterioration begins in the area of the brain that controls memory; however, the phase begins years well before the first symptom appears. The risk of fatality is reduced when Alzheimer's disease is detected early. It employs neuroimaging or central nervous system scanning to directly or indirectly visualize the function, and structure of the brain. Mild cognitive impairment (MCI) is a period that occurs between the normal aging-related decrease in memory and cognition and the increasingly severe dementia-related deterioration. Difficulties with remembering, speech, or judgment may be a symptom of MCI. Dementia brought on by Alzheimer's disease and other brain illnesses may be more probable as a result of MCI. According to the latest figures, there are currently about 46.8 million older people facing this

✉ Rajarshi SinhaRoy
rajarshi921@gmail.com

Anupam Sen
anupam.sen2006@gmail.com

[1] Department of Computer Science, St. Xavier's College (Autonomous), Kolkata, West Bengal 700016, India

[2] Department of Computer Science, Government General Degree College, Singur, West Bengal 712409, India

disease, and 44 million of them have been diagnosed with Alzheimer's disease. By 2050, the population will have risen to 131.5 million. The number of persons with dementia and Alzheimer's disease in India is expected to reach about 7.5 million by 2030. In the medical field, deep learning seems to be a revolutionary technology. Deep learning algorithms are necessary for the medical profession to capture large volumes of clinical information. Deep learning is a type of machine learning that uses neural network models to learn unsupervised from unstructured or unlabeled data. The neural nets are built in the same way as the human brain, containing neuron nodes connected in a web-like pattern. Deep learning algorithms have a number of benefits over traditional machine learning techniques. Deep learning algorithms, as previously discussed, are well suited to working with complex, high-dimensional medical image processing. Recent days have seen the adoption of GAN-based algorithms for a variety of tasks, including automatic segmentation, restoration, and automatic segmentation. This is due to the growth of the GAN. A generator and a discriminator make up a GAN model. Both are trained in opposition to one another, with the generator attempting to produce an artificial image that the discriminator is unable to differentiate from the actual one. In comparison with a traditional auto-encoder, the adversarial strategy in GAN can encourage the discriminator to produce a more realistic image. The GAN technique has been utilized in multiple research publications to forecast future images of the brain, which might be seen as an image synthesis issue. The low resolution of MRI pictures and the lack of real-world data, however, prevented us from getting the accuracy we were hoping for. SRGAN is a GAN-based model that utilizes a perceptual loss function that combines adversarial loss and content loss characteristics to achieve very high resolution for images. DCGAN is a GAN-based model that uses the transposed convolution technique to perform up-sampling that helps more accurate results in a faster time. In this study, we developed the SRGANs approach as an image enhancer task to improve the resolution and the DCGANs method as an image synthesis task to deal with the shortage of MRI datasets. For classification, high-level features from brain images are extracted using a CNN-based architecture. Also, for the classification and forecasting of this disease, we use a CNN-based architecture. We made an effort to examine all the dangers and influences that damage the brain in Alzheimer's disease, and we have looked at magnetic resonance images to better comprehend the condition. The second section contains the related work in this field of research. In part 3, we discussed our datasets, and in part 4, we discussed our methodology, and the methods we used to forecast Alzheimer's illness. We talked about the experiments and results in Sect. 5. Finally, Sect. 6 contains the conclusion.

2 Related Work

For many years, researchers are working in this field using several methods to diagnose this disease. The authors of [1] conducted research to anticipate the disease category. This research suggests a brand-new three-part adversarial network-based AD detection method. BSGAN-ADD combines CNN-based AD detection with a generative adversarial network (GAN)-based brain slice image enhancement. Stacked CNN levels in the generator have been utilized in the prediction step to retrieve high-level brain characteristics via the classification of 2D brain slice pictures. And to produce the probability values of sick states, the classifier receives the retrieved brain features. The authors of [2] want to simultaneously forecast subject-specific improvement in cognitive score and MRI size to forecast illness development in multiple views. So they used two models that two models are combined using three integration procedures. The integrated approach introduces ROI mask and then ROI loss to take advantage of existing expert knowledge of illness progression. Experimental findings on the longitudinal dataset from the Alzheimer's Disease Brain—imaging Initiative, showed that, for the prediction of the cognitive score, the effective system outperformed the separate regression model. In particular, they combined both regression and GAN models and trained them simultaneously, and the outcome was great. In research paper [3], researchers looked at several papers and tried to develop them professionally. Four of the 16 experiments employed both deep learning and conventional machine learning techniques, while 12 used exclusively deep learning techniques. Alzheimer's disease (AD) classification accuracy using conventional ml algorithms was up to 98.8%, while the accuracy for predicting the transition from MCI to AD was 83.7% (AD). For AD classification and 84.2% for MCI conversion prediction, RNN had produced accuracy levels of up to 96.0%. In this publication [4], they demonstrated that the concept of Alzheimer's disease (AD) may be used to generate synthetic images depending on an individual patient's MR image using MR images to forecast changes in the brain. This enables the creation of artificial visuals that express different degrees of the characteristics associated with AD. In the paper [5], the Alzheimer's Disease Neuroimaging Initiative project's standardized MRI datasets are used to validate the suggested methodology. The training of a CNN to recognize the deep learning properties of MCI participants uses age correction, local patches, and structural brain imaging features. To anticipate the AD conversion, features are finally loaded into an advanced machine classifier. This method yields an area mostly under ROC and AUC as well as an accuracy of 86.1% and 79.9%. The suggested CNN-based technique has considerable potential for predicting the conversion of MCI to AD using only MRI data, according to the results.

In paper [6], in addition to performing the diagnosis and forecasting of Alzheimer's disease, an artificial model has been created (AD). It employs a multi-modal 3D CNN classification model. The outcomes demonstrate the feasibility of mapping cerebral tissue's information about the structure and the image's closeness to the genuine thing. In the system [7], they developed for forecasting disease progression consisting of two parts: a 3-dimensional multi-information GAN plus a 3-dimensional DenseNet-based multi-class classification net optimized with a focus loss. A high-quality, one-of-a-kind 3D brain MRI image may be provided on each imaging of the brain via mi-GAN. A 6.04% improvement is seen when conditional GAN and cross-entropy loss are used to compare the performance of pMCI with sMCI. Their mi-GAN performs at the cutting edge with a structural similarity measure of 94.3% between the simulated and actual MRI images. In [8], the very first tier of the 5 suggested systems is in charge of MRI acquisition. The training datasets are improved in the second layer using data mining algorithms and dynamic filtering and in the fourth layer, the CNN architecture was used. On the ADNI dataset, the suggested framework obtained classification accuracy rates of 99.6%, 99.8%, and 97.8%. In paper [9], they suggest a unique method to model the rate at which AD develops and the rate at which the brain ages. By using a sequence of DCGANs to create artificial MR pictures, they aim to do this. After creating the images, they analyze them by estimating the characterizing fractal patterns of the cortical ribboning. Through cascading DCGANs that model various stages of AD, this research illustrates the viability of the proposed solution. A combination of DCGANs that would imitate the various illness stages might be used to prolong the length. Using the cortical ribbon's fractal dimension, atrophy is measured. A declining fractal dimension indicates that the sickness is getting worse with time.

3 Materials

3.1 Dataset and Attributes

We had used Alzheimer's Disease Neuroimaging Initiative (ADNI) depository in our tests since it offers a compendium of common exploration data for Alzheimer's complaint. This database makes the public's MRIs and material individual data of test subjects available. Images of individualizes from multiple visits over a period of roughly 4 to 5 times are included in the data. This gave researchers access to a full range of commonly used research data that they could use to investigate underlying the diagnosis and management of Alzheimer's disease. Very mild demented, mild demented, non-demented, and moderate demented are the four sub-

Table 1 Summarization of the dataset for Alzheimer's disease prediction

Class	AD type	Images
Class-1	Mild demented	896
Class-2	Moderate demented	64
Class-3	Non-demented	3200
Class-4	Very mild demented	2240

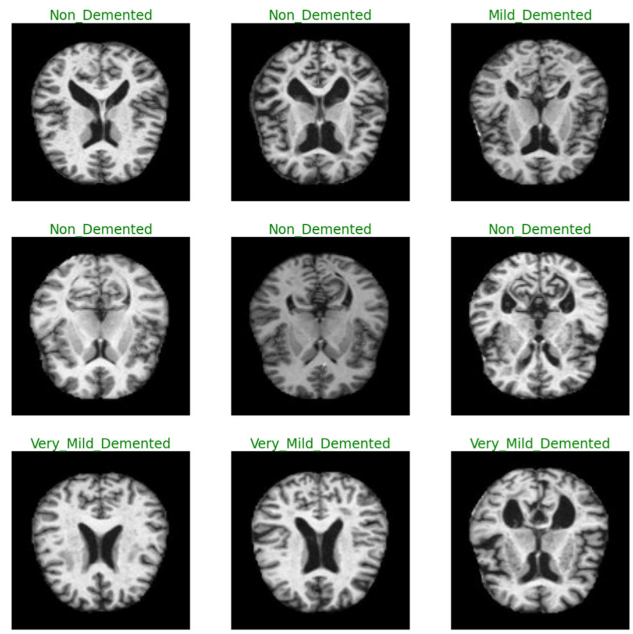

Fig. 1 Random sample of MRI scans from the datasets

folders that make up the data that it provides. The specifics of the information we used are summarized in Table 1 (Fig. 1).

4 Proposed Method

To categorize the illnesses phases, the suggested model makes use of databases. We propose an integrated GAN [10] with deep CNN architecture that enhances classification efficiency by preprocessing and training to categorize Alzheimer's disease (ad) data into multiple stages. By taking into account key risk variables and indeed the techniques we used to forecast Alzheimer's disease [11], we have outlined how we conducted the research. The research method is categorized into 4 main phases: the preparation of the data; the filling in of incomplete data with deep convolutional GANs; the improvement of image resolutions utilizing super-resolution GANs; and the categorization and prediction of diseases with 2D convolutional neural networks. Figure 2 depicts the entire design of the suggested method, while the subsequent sections explain each of the mentioned processes

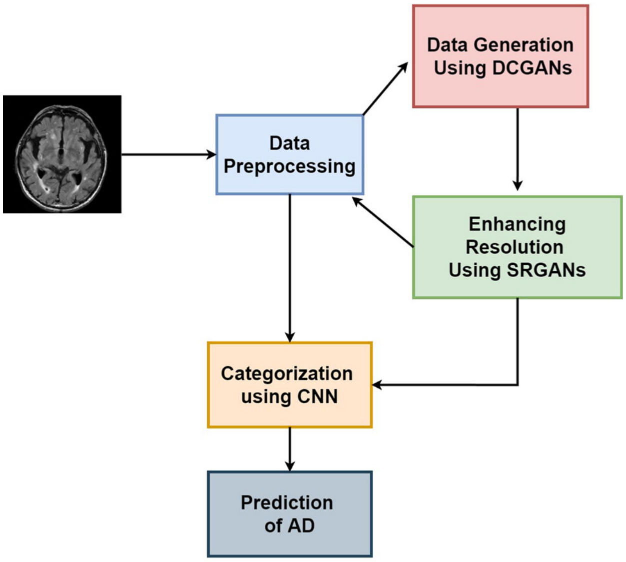

Fig. 2 A simple model of our proposed architecture

Algorithm 1 Data Compilation and Augmentation Algorithm

Require: $Ifile, (w, h),$ ▷ image file, size
Ensure: $Ofile,$ ▷ Output file
$Image \Leftarrow read(Ifile)$
while $i \in Images$ **do**
  $a_i \Leftarrow adaptive\_thresholding(i)$
  if $cropping$ **then**
    $b_i \Leftarrow cropping(i)$
  end if
  if $filtration$ **then**
    $f_i \Leftarrow filtration(i)$
  end if
  $g_i \Leftarrow grayscale(i)$
  $r_i \Leftarrow resize(g, w, h)$
  $Images \Leftarrow r_i$
  if $augmentation$ **then**
    $custom\_augmentation()$
    $newImages \Leftarrow augment(h_i)$
    $Images \Leftarrow newImages$
  end if
end while
store the pre-processed images in the O file
return $Ofile$

individually. Throughout our study, we consider that P^n represents the MRI information for subject n. This model's diagnosis output can be stated as follows:

$$T^n = f(P^n) \tag{1}$$

where T^n represents the anticipated label for the *n*th topic. If somehow the *n*th topic lacks information, then the system will produce synthetic scan data based on its fundamental significance. The model's diagnosis output can be written as:

$$T^n \approx f(P^n) + g(P^n) \tag{2}$$

They both are mapping functions, f and g. The following equation demonstrates two main objectives throughout this approach: (i) developing an appropriate mapping function g for generating the synthetic scan images, which would be covered in subsection "Data Generation Using DCGANs" and (ii) enhancing both the generated and available dataset using SRGANs which is covered in subsection "Data Enhancing Using SRGANs" and (iii) inside the subsection titled "Categorization Using CNNs" a categorization model for both diagnosing and predicting AD is proposed.

4.1 Data Preprocessing

An impact of various people's brain sizes upon that prediction model was removed using a standard data preprocessing technique to ensure the efficiency of our approach and prevent overfitting [12]. Preprocessing is used to create 2D scans from the MRI images. Perhaps every image is $1 \times 128 \times 128$ pixels in size. In Fig. 1, preprocessed pictures from MRI data are displayed. Three sets: a training dataset, a test dataset, and a validation dataset, of the 2D brain component data were created. The individual's brain characteristic image made up 80% of training data obtained using the random selection technique, with the remaining 20% used equally for testing and validation. This was simple to have underfitting and otherwise overfitting issues mostly with the scant amount of visual data available for deep learning. We generated synthetic images using DCGANs to increase the number of training samples; this is given in Fig. 3. The MRI scans' low resolution and lack of details in the images are further factors that affect the model's accuracy. Our model, depicted in Fig. 3, employs the SRGANs to get around this. Additionally, fresh training images were produced using the zero-mean Gaussian noise including a variance of 0.005. Intensity adjustment was the last technique [13]. Steps of 12% were used to adjust the intensity values from 95 to 115%. The majority of cutting edge approaches employ the traditional thresholding operator, which applies a single global threshold to all pixels. Contrarily, under adaptive thresholding, it is adjusted dynamically as the image is being processed. Its adjacent pixel intensity values affect the threshold value for each pixel. The threshold value is computed for each pixel. The result is regarded as a background value if it falls below the threshold; otherwise, it is regarded as a foreground value. Cropping and filtration are the following stages in digital picture processing. The photographs are then generated with a grayscale after the filtering procedure. If the gathered size of the image is not 128×128, a transformer is employed to resize the created photographs to that size. In that case, the data augmentation mechanism is ini-

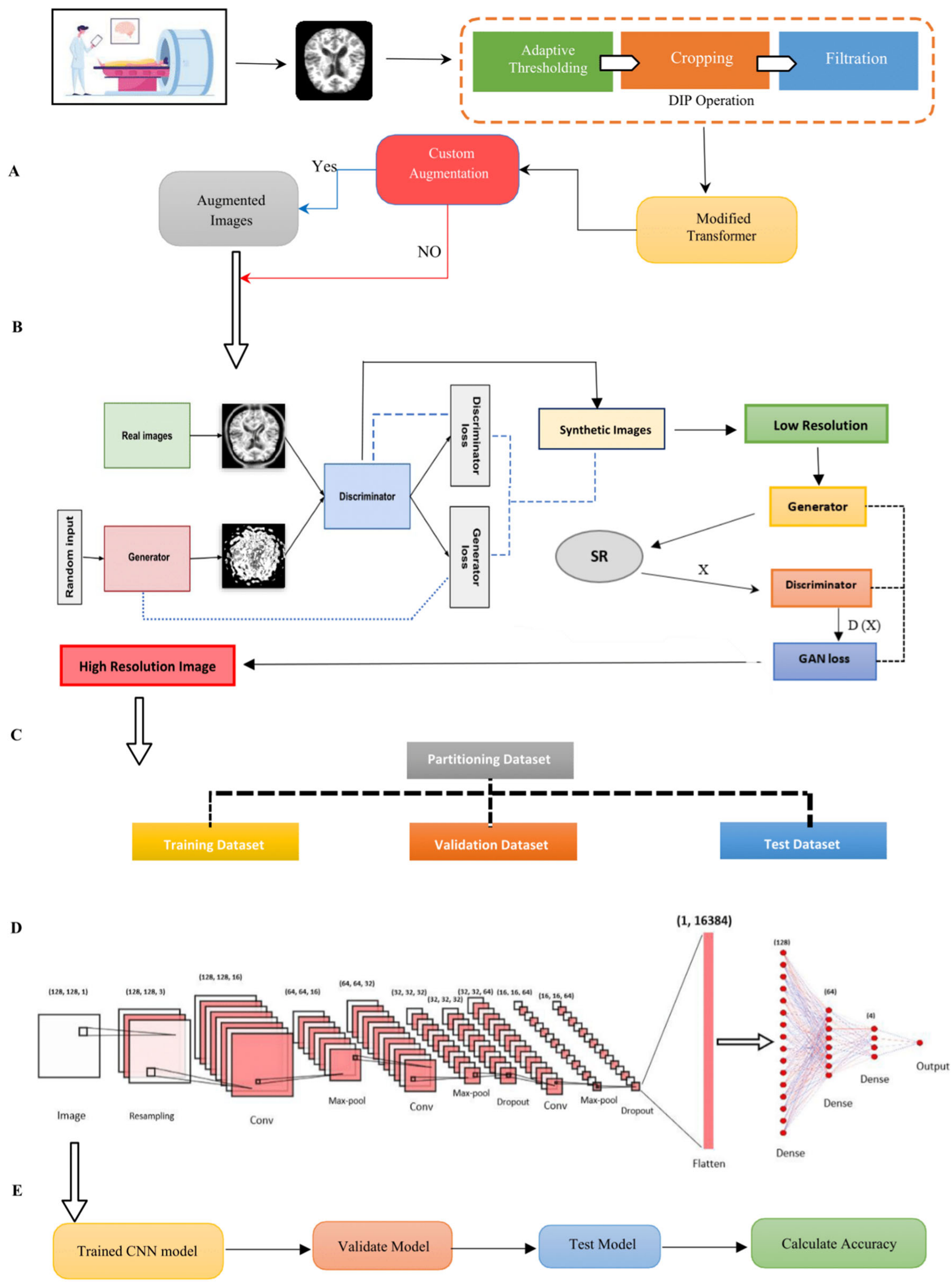

Fig. 3 An illustration of the framework we suggest that combines: **A** a summary of the data preprocessing stages. **B** A generalized model of SRGANs and DCGANs for enhancing picture resolution and creating synthetic images, respectively. **C** Dividing the dataset into a training dataset, a validation dataset, and a test dataset. **D** A description of our end-to-end compact CNN framework. **E** Assessing our model to obtain the prediction

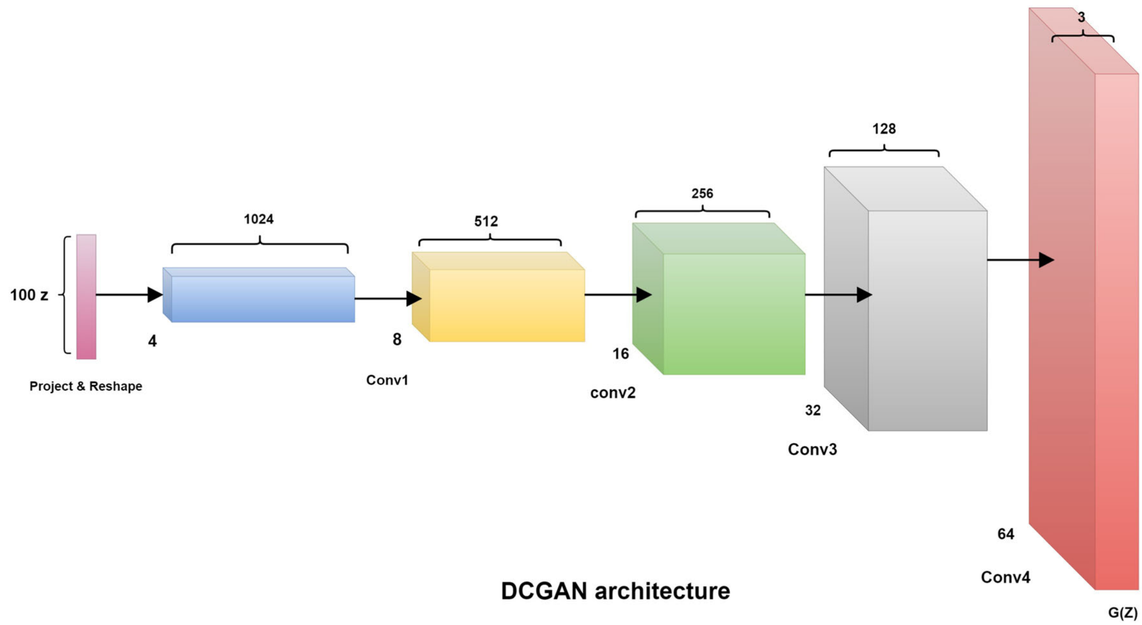

Fig. 4 LSUN image modeling makes use of the DCGAN generator [16]

tialized if it is necessary. The framework uses magnifying, moving, rotating, horizontally tilting, and a number of other augmentation features. In order to strengthen the classifier model, data augmentation assists to create additional [14] and diverse training sets [15].

4.2 Data Generation Using DCGAN

GANs are a type of generative modeling that employs deep learning techniques like convolutional neural networks. A generating model (G) randomly collects the distribution of data, while a discriminative model (D) determines the possibility of similarity that a sample (x) came out from a labeled training dataset [17]. Together, these two adversarial models make up a GAN. To create a probabilistic model N_g given a set of data x and then optimal goal is the generator (G). By translating a pervasive environment $N_p(P)$ toward a feature space $G(x; \theta_d)$, it achieves this. The discriminator, however, $D(x; \theta_d)$, only generates a unique scalar value. This number represents the chance that x originated from the training set as opposed to the produced probability of the distribution of P_g. Discriminator and generator are developed concurrently. Hence, in such an effort to reduce the generating errors $\log(1 - D(G(P))$, the generator updates its weights. To optimize the overall result of $\log(D(x))$, the discriminator D simultaneously attempts to modify its weights.

The DCGAN generator is shown in Fig. 4 from the research article [18]. This layer receives input 100×1 noise vector z and then converts that to the $64 \times 64 \times 3$ $G(Z)$ output. This architecture's initial layer's expansion of the noises is particularly intriguing. Increasing from 100×1 to $1024 \times 4 \times 4$, in this network which is also referred as "project and reshape". We can observe that after this layer, the network is reshaped by the application of the $(N + P - F)/S + 1$ equation that is typically presented with convolutional layers.

$$
\begin{aligned}
&100 \times 1 \Rightarrow 1024 \times 4 \times 4 \Rightarrow 512 \times 8 \times 8 \Rightarrow \\
&\quad 256 \times 16 \times 16 \Rightarrow 128 \times 32 \times 32 \Rightarrow 64 \times 64 \times 3
\end{aligned}
$$

Hence, the loss function of DCGANs is followed by the equation (4) stated below

$$
\begin{aligned}
\text{Loss}(D, G) = {} & E_{x-pdata(x)}[\log(D(X))] \\
& + E_{x-p(x)}[1 - \log(D(G(X)))]
\end{aligned}
\tag{3}
$$

We discuss the artificial data generation strategies used by the method to increase dataset volume while utilizing DCGAN. Figure 5 depicts a summary of system techniques. As in this stage, we employ DCGAN to make artificial pictures of Alzheimer's disease.

4.3 Data Enhancing Using SRGAN

It is challenging to obtain an upscaling factor of nearly 4x for such a bulk of picture images before SRGANs. For producing high-quality, cutting edge images, this suggested SRGAN architecture overcomes the majority of these problems. A tremendously difficult issue is the idea of estimating and producing a high-resolution image out of a low-resolution image. The generator and discriminator are both parts of SRGANs. The low-resolution image data are sent to a Conv layer containing 9×9 kernels by the generator. The next layer is just

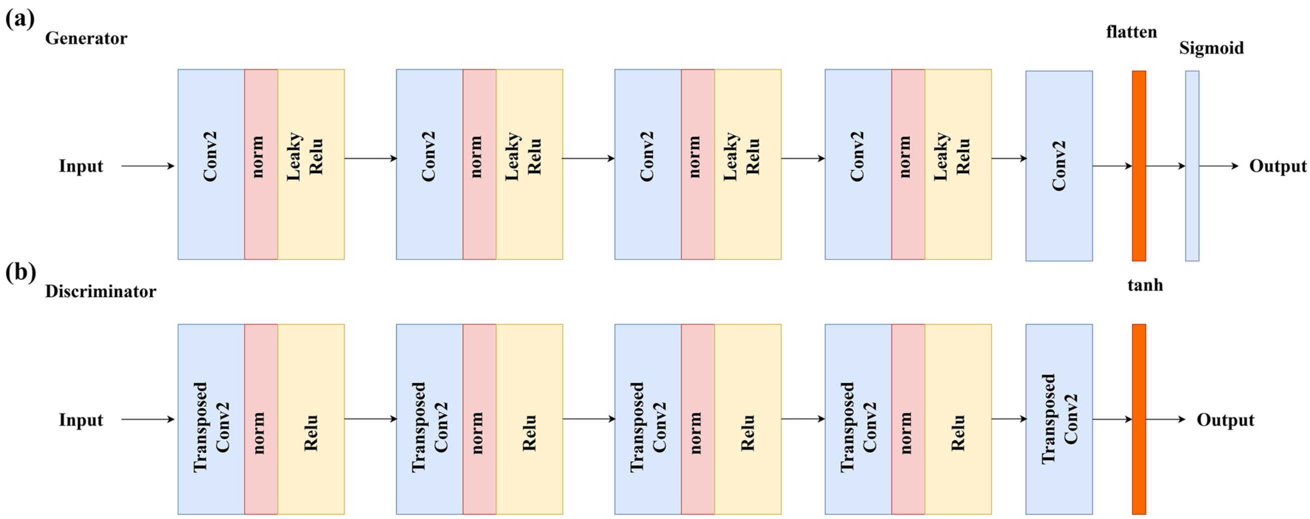

Fig. 5 An architecture of the discriminator and generator of DCGANs. **A** In the discriminator, there are convolution layers with normalize and LeakyReLU for the network and used this network 4 times and then connected with the convolution layer and at the end flatten and Sigmoid layers are used. **B** In the generator, there are transposed convolution layers with normalize and ReLU for the network and used this network 4 times and then connected with transposed convolution layer and at the end, tanh layer is used

a parametric ReLU [19] layer, which is used specifically for projecting low-quality images to high-quality images. There are 16 B residual blocks that ResNet [19] created. Two Conv layers, each with a comparatively tiny 3×3 kernel as well as 64 feature maps, are applied inside this residual block. Batch normalization layers are therefore applied, with parametric ReLU [20] serving as the activation function as well as the elementwise sum approach used to feed-forward the outcome in addition to the jump link outcome to provide the outcome. The generator attempts to create accurate representations of the image to avoid detection by the discriminator, whereas the discriminator searches for misleading pictures. Both discriminator and generator are concurrently getting better and contending with one another. Utilizing LeakyReLU to design DCGANs for activator is comparable to the same discriminator design used for SRGANs.

A Conv layer is followed by LeakyReLU (with 0.2 alpha value) and a set of repeating blocks of Conv layers, followed by the Normalization layer and the LeakyReLU. After 5 sets, there is a dense layer followed by a sigmoid activation function. LeakyReLU [21] (with 0.2 alpha value) as well as a series of repeated sets of Conv layers is preceded by a convolution layer, the normalization layer, and also the LeakyReLU. Following 5 sets, at last, there are dense layers plus a sigmoid activation function. Also, the 8 convolutional layers present in the network contain 3×3 filter kernels, multiplied by 2 to get a range in size of 512 from 64. Among the most frequently employed terminology in the analysis of photographs is the PSNR before that MSE loss has been used. However, rather than more aesthetically noticeable properties like texture detail, these phrases are more focused on identifying the characteristics of each particular pixel. With the aid of the recently developed loss known as perceptual loss, VGG loss suggests a loss that is intended to battle additional perceptually oriented traits [22] (Figs. 6, 7).

$$l^{\mathrm{SR}} = l_x^{\mathrm{SR}} + 10^{-3} l_{\mathrm{Gen}}^{\mathrm{SR}} \tag{4}$$

The mathematical equation for simple content loss is

$$l_{\mathrm{MSE}}^{\mathrm{SR}} = \frac{1}{r^2 W H} \sum_{x=1}^{rW} \sum_{y=1}^{rH} (I_{x,y}^{\mathrm{HR}} - G_{\theta_G}(I^{\mathrm{LR}})_{x,y})^2. \tag{5}$$

Also, the formula for the loss of VGG content is

$$l_{\mathrm{VGG}/i,j}^{\mathrm{SR}} = \frac{1}{W_{i,j} H_{i,j}} \sum_{x=1}^{W_{i,j}} \sum_{y=1}^{H_{i,j}} (\phi_{i,j}(I^{\mathrm{HR}})_{x,y} - \phi_{i,j}(G_{\theta_G}(I^{\mathrm{LR}}))_{x,y})^2 \tag{6}$$

and for adversarial loss, the mathematical formula is

$$l_{\mathrm{Gen}}^{\mathrm{SR}} = \sum_{n=1}^{N} -\log D_{\theta_D}(G_{\theta_G}(I^{\mathrm{LR}})) \tag{7}$$

Such loss is favored over the MSE loss because it is concerned to enhance the image quality rather than comparing the pictures pixel by pixel. As a result, researchers can get improved outcomes with the SRGAN model by applying such a loss function [24]. Also, the discriminator loss is the

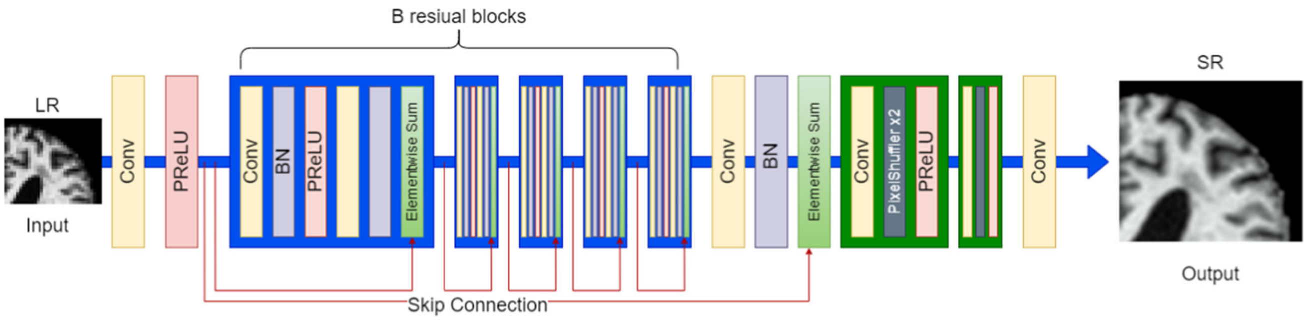

Fig. 6 An architecture of the generator of SRGANs [23]

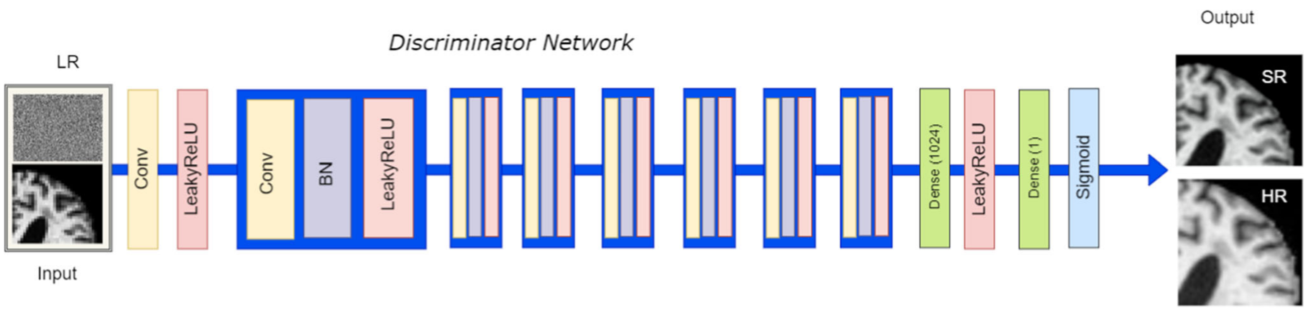

Fig. 7 An architecture of the discriminator of SRGANs [23]

Table 2 Summarization of the major activation functions and its mathematical formula

Activation function	Mathematical formula
ReLU	$f(x) = \begin{Bmatrix} x, & x > 0 \\ 0, & x \le 0 \end{Bmatrix}$
Tanh	$f(x) = \tanh x = \frac{e^x - e^{-x}}{e^x + e^{-x}}$
Sigmoid	$f(x) = \sigma = \frac{1}{1+e^{-x}}$
Softmax	$f(x) = \sigma = \frac{e^{x_i}}{\sum_{j=1}^{k} e^{x_i}}$
LeakyReLU	$f(x) = \begin{cases} x, & x > 0 \\ \alpha x, & x \le 0 \end{cases}$

same as GANs discriminator loss function

$$\min_{\theta_G} \max_{\theta_D} \mathbb{E}_{I^{HR} \sim p_{\text{train}}(I^{\text{HR}})} \left[\log D_{\theta_D} \left(I^{\text{HR}} \right) \right] + \mathbb{E}_{I^{\text{LR}} \sim p_G(I^{\text{LR}})} \left[\log \left(1 - D_{\emptyset_D} \left(G_{\emptyset_G} \left(I^{\text{LR}} \right) \right) \right) \right] \tag{8}$$

4.4 Categorization Using CNN

There are three convolutional layers, three max-pooling layers, one rescaling layer, one flatten layer, two dropout layers, and three dense layers in our CNN model [25]. The several functions like activation, loss, optimization, etc., are just a couple of the variables that affect the network. The research employs a variety of combinations for all these parameters.

To tackle complicated problems [26] and to improve the neural network's efficiency for expression, the activation function is used. We have presented a few incredibly efficient activation functions and their conceptual formulas in Table 2. We use the sigmoid and ReLU as activation functions in our research. In our neural network, we used rescaling the image collected as an input. A dropout layer was then followed by two sets of convolution layers, a max-pooling layer, and so forth: convolution layer again, then max-pooling layer, then dropout layer. One flatten layer is followed by three dense layers. [27]

$$\begin{aligned} &128 \times 128 \times 3 \Rightarrow 128 \times 128 \times 16 \Rightarrow 64 \times 64 \times \\ &16 \Rightarrow 64 \times 64 \times 32 \Rightarrow 32 \times 32 \times 32 \Rightarrow 32 \\ &\times 32 \times 32 \times 32 \times 32 \Rightarrow 32 \times 32 \times 64 \Rightarrow 16 \times \\ &16 \times 64 \Rightarrow 16 \times 16 \times 64 \Rightarrow 1 \times 1 \times 1638 \Rightarrow \\ &1 \times 1 \times 128 \Rightarrow 1 \times 1 \times 64 \Rightarrow 1 \times 1 \times 4 \end{aligned}$$

In Fig. 8, we have shown the 2D architecture of our proposed CNN network. As a convolution filter, a 3×3 kernel is utilized, along with "Same" padding. Additionally, we used the Adam optimizer to finalize CNN model optimization (Table 3).

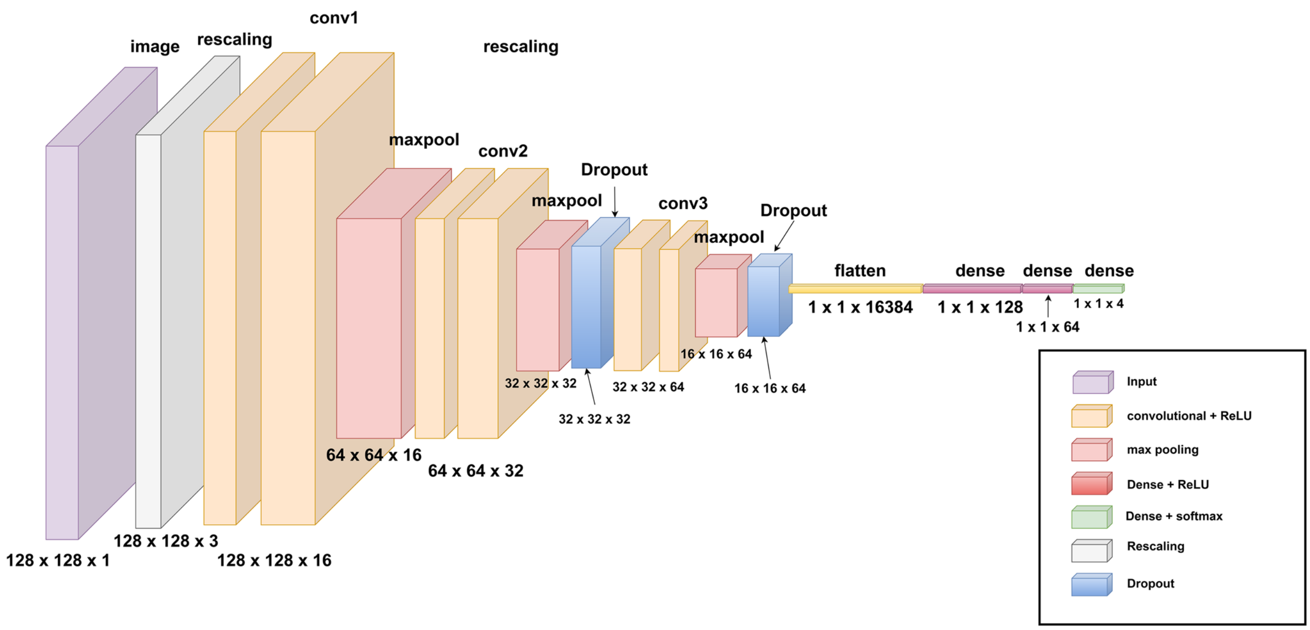

Fig. 8 An illustration of our proposed CNN architecture

Table 3 Parameters for our CNN model

Layer (type)	Param
Convolution layer 1	448
Convolution layer 2	4640
Convolution layer 3	18,496
Dense layer 1	2,097,280
Dense layer 2	8256
Dense layer 3	260

5 Experiments and Results

Throughout our approach, we develop data generation using DCGANs, enhancing both the generated and available dataset using SRGANs. In the end, we used our proposed model.

5.1 Experiment Environment

Our studies were carried out on Google Colab, which provides 68.40 GB of storage space, and 25.51 GB of RAM, with a GPU backend. The deep network algorithms are implemented using the Keras package and the coding language used is Python.

Convolutional layers use kernel sizes of 3×3, while max-pooling layers use kernel sizes of 2×2. Both 2nd and 3rd convolutional layers are followed by a dropout layer, which is done with 0.20 and 0.25. For the output and hidden layer, correspondingly, ReLU and Softmax were utilized as activation functions [28].

5.1.1 Experiment Matrix

To assess the effectiveness of AD detection, the usual metrics were applied. Accuracy (ACC), precision, recall, and F1-score are used to describe these measurements. Here, the amounts of true positives (TPs) and false positives (FPs) are given.

$$\mathrm{ACC} = \frac{\mathrm{TP} + \mathrm{TN}}{\mathrm{TP} + \mathrm{TN} + \mathrm{FP} + \mathrm{FN}} \tag{9}$$

$$\mathrm{RECALL} = \frac{\mathrm{TP}}{\mathrm{TP} + \mathrm{FN}} \tag{10}$$

$$\mathrm{PRECISION} = \frac{\mathrm{TP}}{\mathrm{TP} + \mathrm{FP}} \tag{11}$$

$$\mathrm{F1} = 2 * \frac{\mathrm{RECALL} * \mathrm{PRECISION}}{\mathrm{RECALL} + \mathrm{PRECISION}} \tag{12}$$

Let FP and FN stand for true and false negatives, respectively. Also, the region under the ROC curve was utilized to measure the categorization performance (AUC). False-positive rate (FPR) is the accurate and correct rate, and true-positive rate (TPR) is just the variance of the ROC curve (TPR).

$$\mathrm{TPR} = \frac{\mathrm{TP}}{\mathrm{TP} + \mathrm{FN}} \tag{13}$$

$$\mathrm{FPR} = \frac{\mathrm{FP}}{\mathrm{FP} + \mathrm{TN}} \tag{14}$$

Table 4 Efficacy of four classifications using the proposed methodology

Approach	Modalities	NL/AD/MCI	NL/AD	NL/MCI	AD/MCI	Param
Magnin et al. [35]	MRI	–	0.902	–	–	–
Ben Ahmed et al. [36]	MRI	–	0.854	0.722	0.663	–
Khvostikov et al. [37]	PET + MRI	0.852	0.885	0.877	0.831	0.17 M
Li et al. [29]	MRI	0.867	0.907	0.893	0.848	4.51 M
Korolev et al. [38]	MRI	–	0.823	0.782	0.751	2.14 M
Hosseini-Asl et al. [30]	MRI	0.824	0.972	0.968	0.867	457.0 M
Suk et al. [31]	PET + MRI	0.915	0.942	0.936	0.912	0.7 M
Wang et al. [32]	MRI	0.975	0.988	0.984	0.936	5.3 M
Feng et al. [33]	MRI	0.957	0.991	0.989	0.894	221.5 M
Emtiaz et al. [34]	MRI	–	0.978	–	–	2.0 M
Our proposed method	MRI	0.997	1.000	0.994	0.995	2.13 M

5.1.2 Performance Comparison

We assessed every specific model's classification technique for our proposed Alzheimer's disease diagnosis model and a number of widely used Alzheimer's disease classifiers in order to assess the efficacy of non GAN-based models. Table 4 displays the research's findings. In experiments on four distinct classification techniques (NL/AD/MCI categorization, NL/AD categorization, NL/MCI categorization, and AD/MCI categorization), our model outperformed all competing approaches. Also, due to the strong modeling versatility that deep structures bring, deep learning-based techniques [29–34] perform more effectively than standard classification methods [35, 36]. With deep learning approaches, the computing expense associated with our suggested model is also minimal when compared to the model's parameters. Our suggested model, however, performs with the maximum level of precision in both the NL/MCI and AD/MCI classifications, demonstrating the capability of our AD prediction model to recognize MCI data and enhance the efficiency of AD clinical prediction. The suggested model has been further contrasted against four neural network-based approaches [29–31, 37] using various training data ratios. To be more precise, we saved 15% of the data to test for each cycle while arbitrarily selecting 85% of them as the training set. Figure 9 displays the variations in several evaluation metrics. Figure 9 in particular displays the variations in precision, recall, and F1 values for the AD groups of the test dataset, correspondingly. The quantitative research on the accuracy, as well as training loss for several AD detection techniques, is displayed in Fig. 10. Table 4 demonstrates that, for whatever proportion of the total dataset is used as training data, our suggested AD detection approach beats all other different algorithms. Furthermore, it was discovered that the suggested model's categorization outcomes will be evaluated because the percentage of training sets rose. The research results additionally demonstrated that the suggested model maintained excellent accuracy in categorization even with a limited amount of training data.

Also, we subsequently explored the effectiveness of AD classification techniques utilizing different GAN architectures for GAN-based method performance comparison. This categorical AD categorization problem was addressed by nine distinct GAN-based AD detection algorithms. In particular, AD recognition algorithms have been developed using 4 distinct primary GAN frameworks: DCGAN, WGAN, Conditional-GAN, and AEGAN. To examine the impact of various GAN architectures on AD classification accuracy, various GAN-based approaches were compared with our suggested model. Table 5 presents the classification results utilizing various GAN architectures. It is indeed clear that GAN performs better in this classification task when used as a high-level brain feature selection technique to produce hidden patterns as well as transmit those to the DNN-based classifier as opposed to using it directly to assess the distribution difference in AD data. The integration of segment position data into the GAN-based AD classification algorithm will increase the precision of the categorization model, according to a comparison of the differences in outcomes between the DCGAN-based and the Conditional-GAN-based classification models.

The significant differences between the encoder–decoder generative adversarial network SL classification algorithm and the AEGAN-TCA-based AD prediction model demonstrated that the framework will retrieve further representative hidden patterns if classification loss is added to the loss computation of the generator. The potential issues among the DCGAN-based as well as WGAN-based recognition models are compared, and the results demonstrate that the performance of the classifier is not considerably improved by utilizing multiple optimization techniques to evaluate the distribution gap between produced information and actual data.

It is demonstrated that DCGAN and SRGAN can greatly enhance the efficiency of the method as well as that prepro-

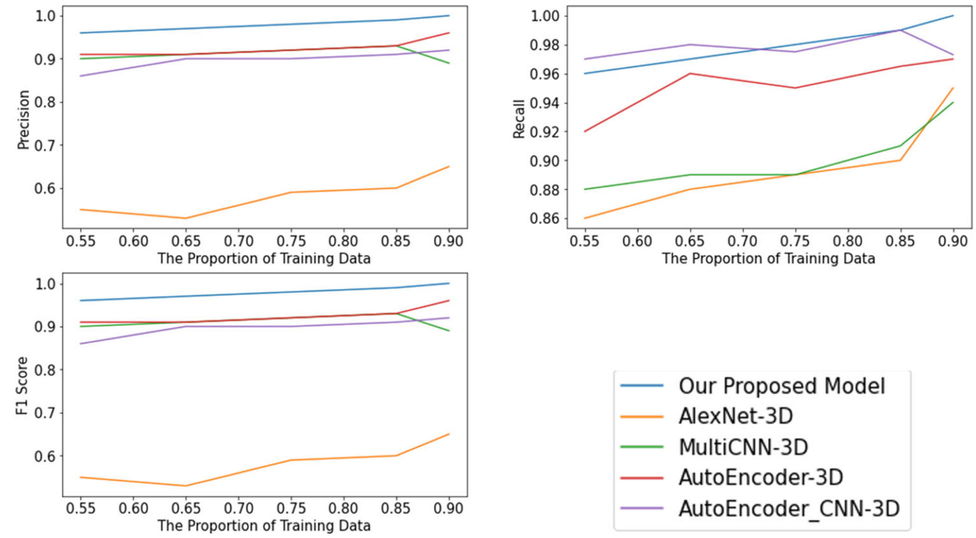

Fig. 9 The precision, recall, and F1 values changed data from a typical testing group as training data proportions changed over time ranging from 55% to 90% for various approaches

Table 5 Several GAN-based AD detecting algorithms' classification results based on supervised, unsupervised learning and TCA

Approach	Precision	Recall	F1-score
DCGAN-SL	0.615	0.578	0.596
DCGAN-USL	0.550	0.562	0.557
WGAN-SL	0.705	0.615	0.665
WGAN-USL	0.545	0.536	0.541
Conditional-GAN-SL	0.718	0.712	0.715
Conditional-GAN-USL	0.708	0.685	0.697
AEGAN-SL	0.852	0.908	0.875
AEGAN-USL	0.739	0.727	0.734
AEGAN-TCA	0.908	0.925	0.918
Our proposed method (no preprocessing)	0.843	0.869	0.856
Our proposed method (no DCGAN and SRGAN)	0.797	0.801	0.815
Our proposed method (no DCGAN)	0.865	0.872	0.884
Our proposed method (no SRGAN)	0.932	0.954	0.954
Our proposed method	0.997	0.998	0.997

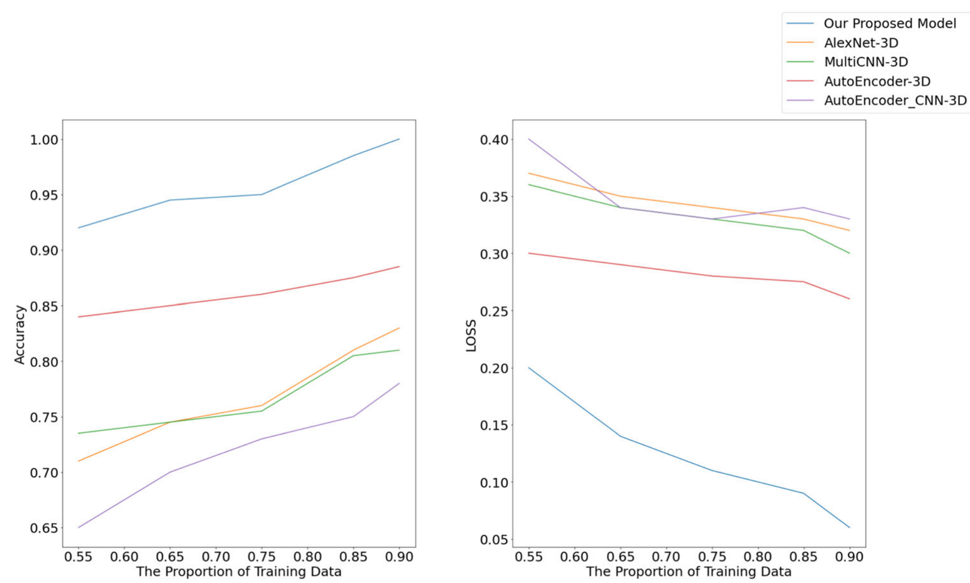

Fig. 10 The accuracy and categorization loss values changed as training data proportions changed over time, ranging from 55% to 90% for various approaches

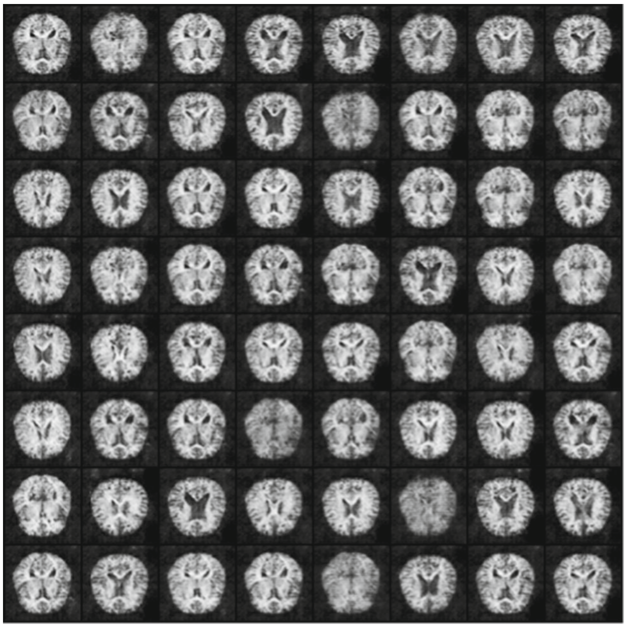

Fig. 11 Result of generating the image using DCGANs after 100 epochs

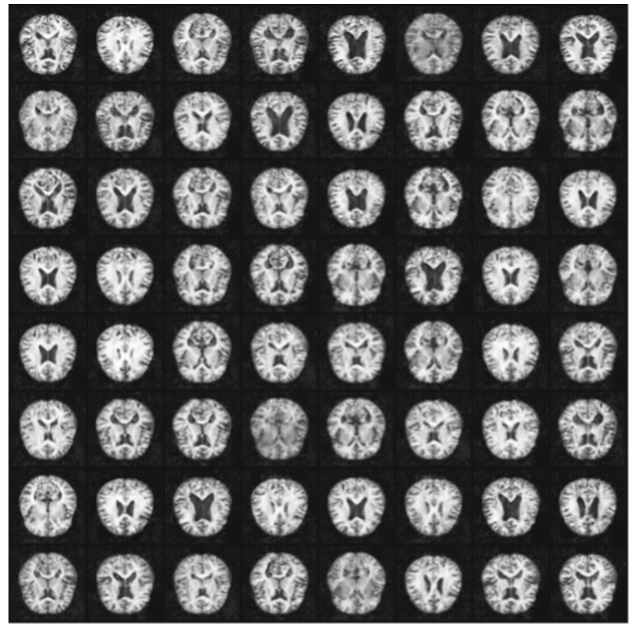

Fig. 12 Result of generating the image using DCGANs after 500 epochs

cessing and SRGAN could indeed direct the model to more effectively retrieve high-quality hidden patterns by making comparisons of the differences in performance in between proposed systems with no preprocessing, no DCGAN, no SRGAN and no DCGAN, no SRGAN, respectively. The two-dimensional characteristic image enhancement method used by the proposed AD classification algorithm is integrated with classification feedback loops to perform categorization improvement of cerebral segment images. The classification of cerebral segment images will typically contain brain features that are simpler for the classifier to properly identify, making our proposed model perform better than other formal GAN-based AD classification approaches.

5.2 Results of Image Generation

In our experiment, we used the batch set of images to generate the batch of synthetic images. The practical accuracy of our model is very good. We achieve 99.4% accuracy. For this accuracy, we get very realistic synthetic MRI images. In Fig. 10, we have shown synthetic images, obtained from DCGANs [29] (Figs. 11, 12, 13).

These generated synthetic images are used to handle the less data problem. In our final output, we can get that this gives excellent results for our total model [21–23]. The accuracy score of our DCGAN model is pretty accurate. And the loss is very low as both shown in Fig. 14.

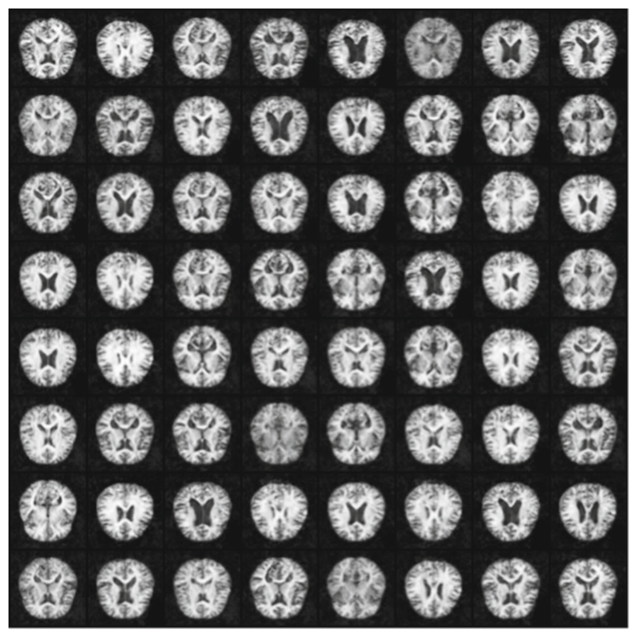

Fig. 13 Result of generating the image using DCGANs after 1500 epochs

5.3 Results of SRGANs in Image

SRGANs highlighted the feature of the images which help the model to understand the disease much better than without the use of SRGANs.

During the research, we discovered that SRGAN can increase the accuracy of the following CNN architecture, allowing CNN to gain good characteristics for compre-

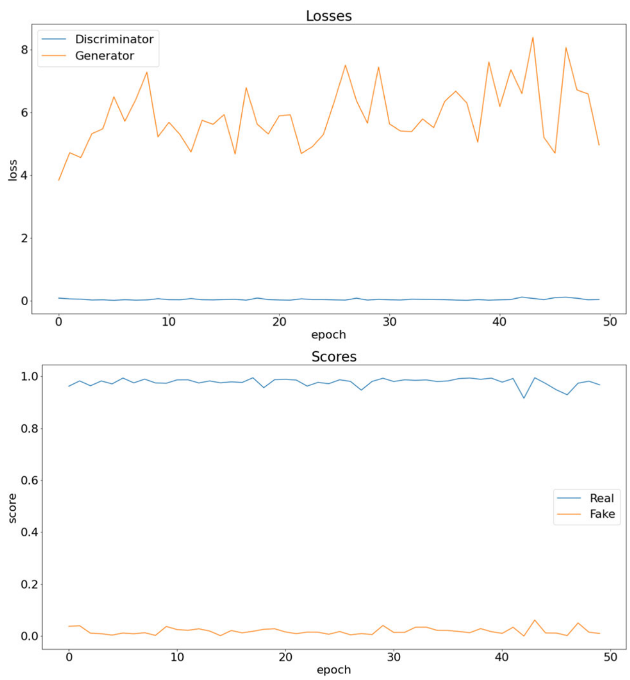

Fig. 14 Result of loss and score of model for generating the image

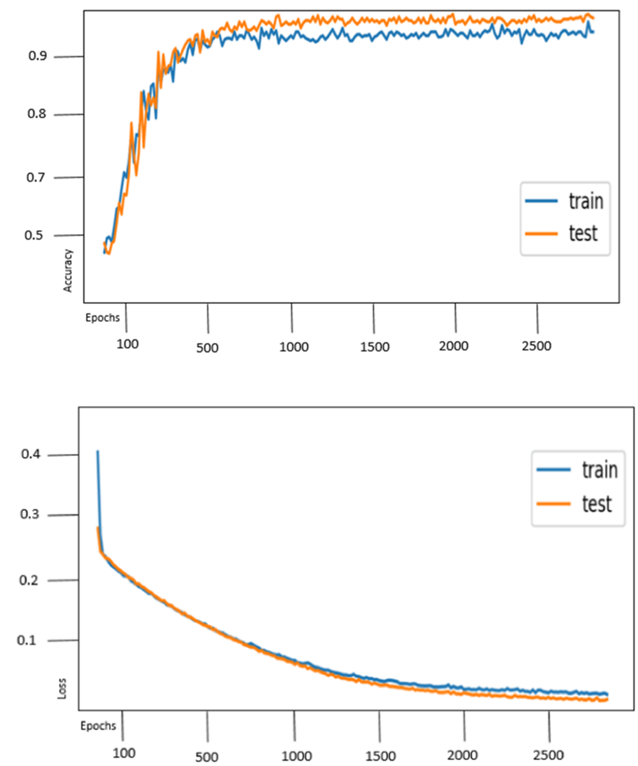

Fig. 16 A graph plot for the accuracy and loss of SRGANs

hending the image. The perceived quality of super-resolved pictures instead of computing performance was the primary priority of this effort [29]. Particularly significant when attempting to provide photo-realistic answers to the SR issue loss function plays an important part. Loss is like a neural network's forecast inaccuracy. The loss function is just the name of the procedure used to compute the loss. For SRGAN, in our studies, we used the "Sparse Categorical Crossentropy" as a loss function.

5.4 Ablation Study

In both clinical and psychological studies, an ablation study is a technique that involves surgically removing an organ, tissue, or other portion of a biological system and examining how the organism behaves without it in hopes of investigating its significance and purpose. In the sense of machine learning, researchers describe an ablation study as a methodical investigation into the efficiency of such a machine learning framework by eliminating a few of its constituent parts. These fundamental elements include things like dataset characteristics and model parts, but an ablation study can also include an entire system or design decisions. Despite the fact that ablation research has typically been insufficient to make inferences about the impact of various modules, it ought to be

Fig. 15 Result of SRGANs in the image

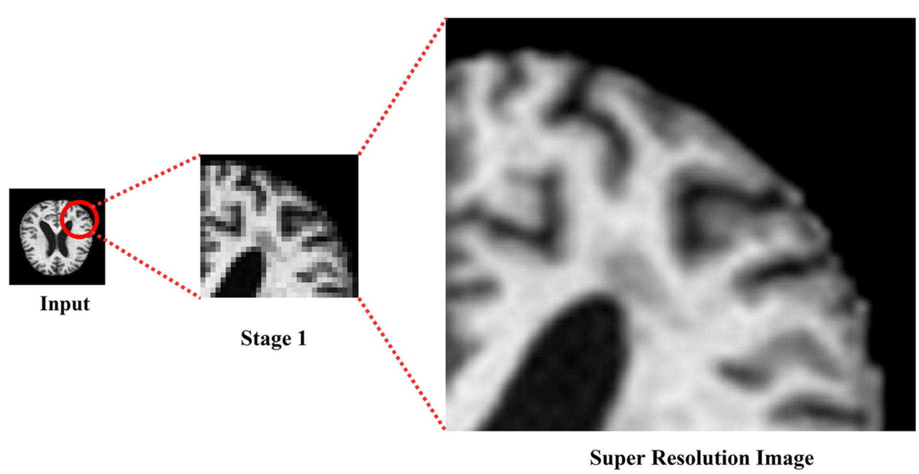

mentioned that when utilized in conjunction with some other scientific and mathematical techniques, it can offer specialists and scholars insightful information. We experimented on Maggy as well as used our own methods to comprehend the ablation study of the model we had suggested. Using SRGANS and DCGANs, we first comprehend the feature ablation experiment by removing some features without first preprocessing the data, and then, we assess the model. The below table explained that preprocessing is necessary for SRGANs and DCGANs to attain proper accuracy.

Second, we omit some of the hidden layers from the deep neural network and evaluate the model in order to comprehend the model ablation experiments. Yet again, the outcomes do not match what the model predicted; in comparison with the suggested model, the loss is substantial and the precision is poor.

Three convolutional layer sections and one dense layer section make up the four basic building blocks of the deep neural network we suggest. For ablation studies, we omit the 1st convolutional layer section and evaluate it as Model 1. For models 2 and 3, we omit the 2nd and 3rd convolutional layer sections, and finally, for model 4, we omit the dense layer section.

Additionally, we have used the Maggy API and LOCO to analyze the ablation experiments (leave one component out). Here, we recognize that the final dense layer portion and the first convolutional layer section play a significant role in accuracy.

5.5 Results of Classification Using CNN Model

Numerous tests are conducted under this classification using the CNN section to determine the optimal answer under the considerations of learning rate and activation function.

In the first investigation, we want to figure out the best learning rate for accuracy. There are very various rates of learning. Our research led us to the conclusion that a learning rate = 0.001 produced the highest accuracy among learning rates varying from 0.05 to 0.0005. The activation function should be studied as the second parameter. The investigations look at two distinct Softmax and ReLU functions. The suggested model delivers better results than most cutting edge systems. The precision is 0.997% higher than the maximum value (Figs. 15, 16, 17).

In Fig. 18, we can understand that the model is giving a great accuracy (near about 1) and very low loss for 100 epochs. This is for both training and validation of the data. Our proposed CNN model gives a proper opposite of accuracy and loss line graph using training data as shown in Fig. 18. In our model, we used sparse categorical cross-entropy as a loss function

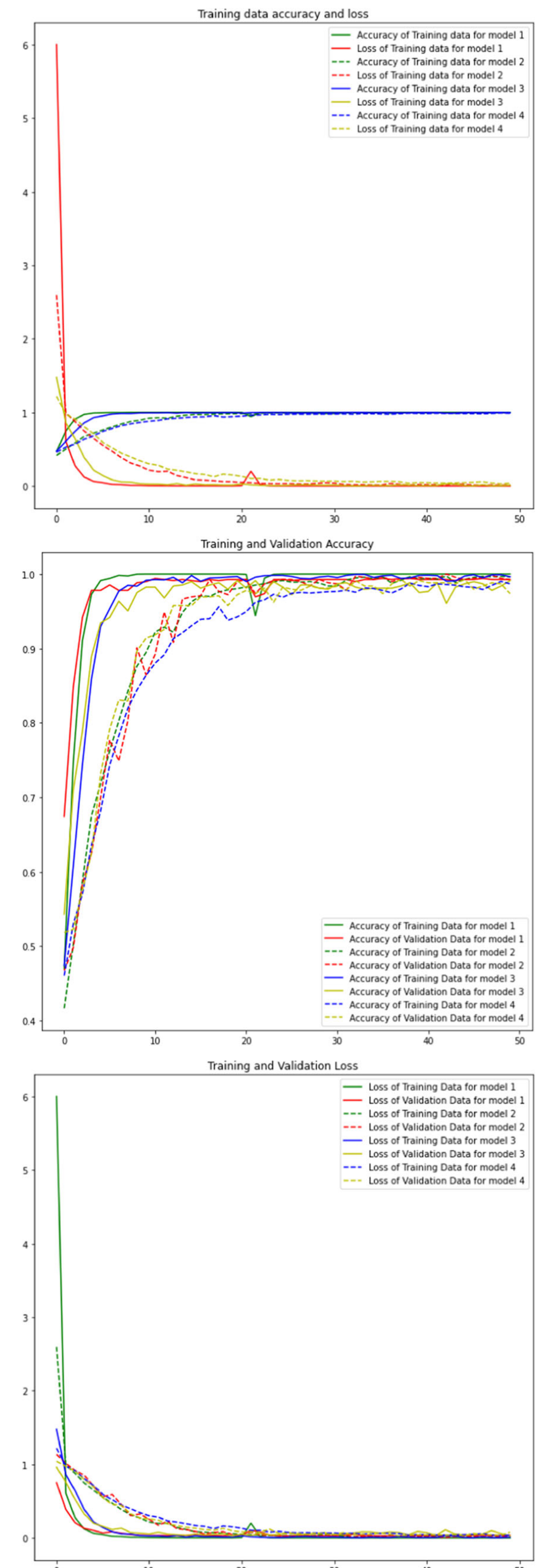

Fig. 17 A graph plot for the accuracy and loss of training and validation of our model to study ablation experiment

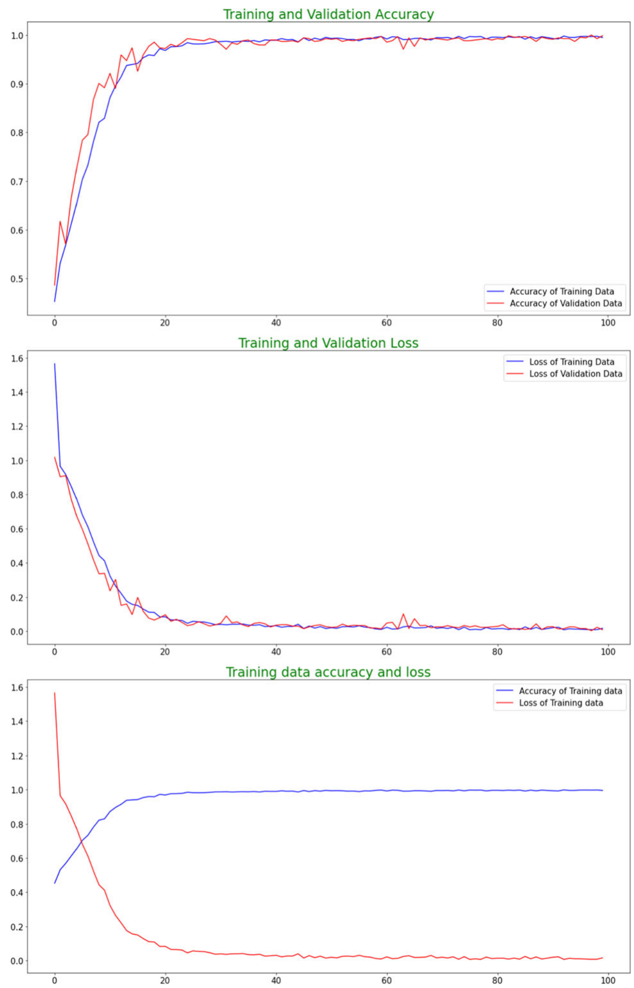

Fig. 18 A graph plot for the accuracy and loss of training and validation of our model

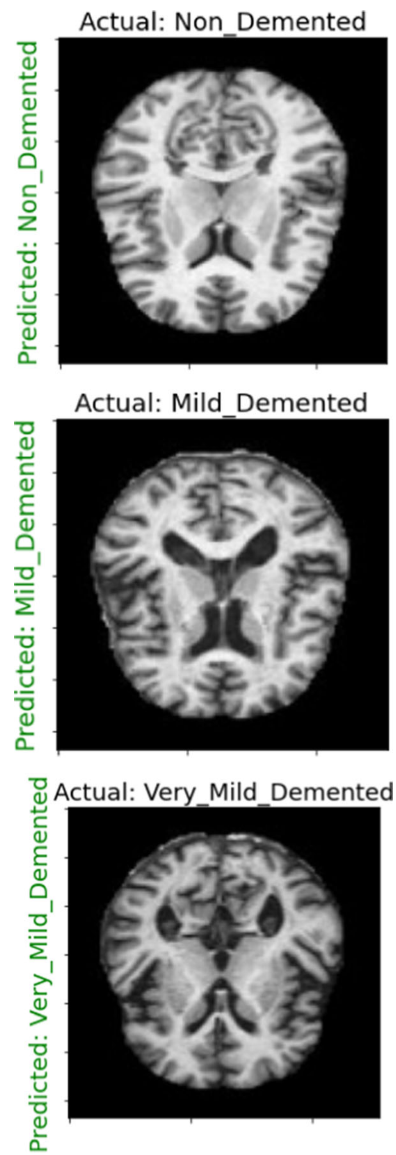

Fig. 19 An illustration of classifications of AD predicted by our model

$$\mathrm{CE} = -\sum_{i=1}^{C} t_i \log f(f(s)_i) \tag{15}$$

In Figs. 19 and 20, the black color type indicates the MRI picture's actual categorization, whereas the green color font represents the classification that our model predicted for the MRI image (Tables 6, 7).

5.6 Discussion

Finally, we suggested a strategy for dealing with the low data, increasing the image resolution and classifying the images with CNN. To correctly classify AD Disease prediction, we have indeed introduced a unique CNN design [30, 39, 40]. Additionally, we examined how synthetic data affected the categorization performance for AD.

Five layers make up the architecture; the very first layer takes care of picture preprocessing, which contains adaptive thresholding as well as data augmentation used to improve training datasets. A generalized version of SRGANs and DCGANs for improving the resolution of the image and producing synthetic data, respectively, is present in the second layer. The cross-validation method is employed to build the CNN in the third step. To prevent overfitting, cross-validation finds the optimal values again for trainable parameters. The CNN architecture is used before the last tier. In our CNN model, there are two dropout layers, two rescaling layers, one flatten layer, three dense layers, three max-pooling layers, and three convolutional layers. The categorization procedure is carried out using a variety of techniques in the final tier. In this study, we explain that now the system is affected by a number of factors, including activation, loss, optimization, etc.

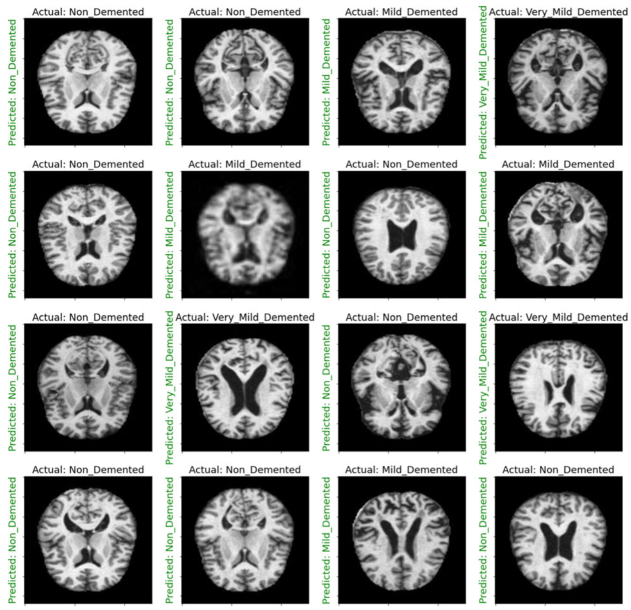

Fig. 20 An illustration of classifications of AD predicted by our model

Table 6 Results analysis of ablation study

Type	Accuracy (%)
Without data preprocessing	74.3
Without DCGAN and SRGAN	78.9
Without DCGAN	84.6
Without SRGAN	93.2
With DCGAN and SRGAN	99.7

Table 7 Results analysis of ablation study for model

Type	Accuracy (%)
1st and 2nd Conv layer with dense layer	96.7
2nd and 3rd Conv layer with dense layer	89.5
1st and 3rd Conv layer with dense layer	95.8
All Conv layer with no dense layer	90.2

Additionally, the Adam optimizer was utilized to generate an optimized model. More studies in the multi-classification domain must be carried out in the future, as well as GANs model's optimization. The optimal outcome may also be attained by employing the 3D network.

6 Conclusion

By generating missing values, we evaluated the effect of the experimental data on the classification task of AD. MRI images were used in the experiment to assess the effects of synthetic data using our suggested methodology. The ADNI dataset experiments show that our technique produces accurate neuroimages. The outcomes of the study also allow us to draw the following three main observations: First, we can see that while it is challenging to map the metadata, for instance, the cranium of the MR picture from the PET image, brain tissue could be projected well in terms of its structural and physiological information. In order to feed more relevant brain characteristics into the DCNN-based classifier and increase the probability of AD, it is also necessary to carry out GAN-based brain image enhancement. Our approach demonstrated a considerable detection performance improvement on real-world datasets when compared to many conventional AD detection techniques. Third, our approach may considerably enhance the accuracy of AD diagnosis and MCI transition prediction when such data are missing. In the near future, revolutionary deep-learning approaches using neuroimaging for the disciplines of primary care, medicine, and public health are likely to benefit from the present advancements in illness diagnostic technology and data-intensive medical science. As a result, within the next few years, both the wider populace and government agencies will need to address current problems and new ones in a serious manner. Once future large-scale research studies are capable of fully evaluating the pertinent novel neuroimaging aspects, the treatment and forecasting of AD regarding deep learning methods with neuroimaging might materialize for targeted therapies in personalized medicine in the upcoming decade.

Acknowledgements We sincerely acknowledge the editor as well as the reviewers for their insightful comments that helped to enhance the manuscript. The Alzheimer's Disease Neuroimaging Initiative shared the data for this investigation.

Author Contributions RS led the implementations, data preprocessing, formal analysis, and experiments, wrote the original manuscript, and revised the manuscript. AS supervised and managed the research. RS contributed to the article and approved the submitted version.

Funding This research was self-funded.

Declarations

Conflict of interest The authors declared that they have no conflicts of interest in this research. The authors certify that they are free of any known financial conflicts of interest or close personal ties that might have looked to have affected the research presented in this study.

References

1. Bai, T.; Du, M.; Zhang, L.; Ren, L.; Ruan, L.; Yang, Y.; Qian, G.; Meng, Z.; Zhao, L.; Deen, M.J.: A novel Alzheimer's disease detection approach using GAN-based brain slice image enhancement. Neurocomputing **492**, 353–369 (2022). https://doi.org/10.1016/j.neucom.2022.04.012

2. Zhao, Y.; Ma, B.; Che, T.; Li, Q.; Zeng, D.; Wang, X.; Li, S.: Multi-view prediction of Alzheimer's disease progression with end-to-end integrated framework. J. Biomed. Inform. **125**, 103978 (2021). https://doi.org/10.1016/j.jbi.2021.103978
3. Jo, T.; Nho, K.; Saykin, A.J.: Deep learning in Alzheimer's disease: diagnostic classification and prognostic prediction using neuroimaging data. Front. Aging Neurosci. **11**(2), 220–234 (2019). https://doi.org/10.3389/fnagi.2019.00220
4. Bowles, C.; Gunn, R.; Hammers, A.; Rueckert, D.: Modelling the progression of Alzheimer's disease in MRI using generative adversarial networks. In: Proc. SPIE, vol. 10574, p. 105741 (2018). https://doi.org/10.1117/12.2293256
5. Lin, W.; Tong, T.; Gao, Q.; Guo, D.; Du, X.; Yang, Y.; Guo, G.; Xiao, M.; Du, M.; Qu, X.: Convolutional neural networks-based MRI image analysis for the Alzheimer's disease prediction from mild cognitive impairment. Front. Neurosci. **12**(777), 1–13 (2018). https://doi.org/10.3389/fnins.2018.00777
6. Lin, W.; Lin, W.; Chen, G.; Zhang, H.; Gao, Q.; Huang, Y.; Tong, T.; Du, M.: Bidirectional mapping of brain MRI and pet with 3D reversible GAN for the diagnosis of Alzheimer's disease. Front. Neurosci. **15**(6013), 1–13 (2021). https://doi.org/10.3389/fnins.2021.646013
7. Zhao, Y.; Ma, B.; Jiang, P.; Zeng, D.; Wang, X.; Li, S.: Prediction of Alzheimer's disease progression with multi-information generative adversarial network. IEEE J. Biomed. Health Inform. **25**(3), 711–719 (2021). https://doi.org/10.1109/JBHI.2020.3006925
8. AbdulAzeem, Y.; Bahgat, W.M.; Badawy, M.: A CNN based framework for classification of Alzheimer's disease. Neural Comput. Appl. **33**(16), 10415–10428 (2021). https://doi.org/10.1007/s00521-021-05799-w
9. Roychowdhury, S.; Roychowdhury, S.: A modular framework to predict Alzheimer's disease progression using conditional generative adversarial networks **2**, 1–8 (2020). https://doi.org/10.1109/IJCNN48605.2020.9206875
10. Radford, A.; Metz, L.; Chintala, S.: Unsupervised representation learning with deep convolutional generative adversarial networks **1**, 1–16 (2015). https://doi.org/10.48550/ARXIV.1511.06434
11. Ledig, C.; Theis, L.; Huszar, F.; Caballero, J.; Cunningham, A.; Acosta, A.; Aitken, A.; Tejani, A.; Totz, J.; Wang, Z.; Shi, W.: Photo-realistic single image super-resolution using a generative adversarial network **12**, 105–114 (2017). https://doi.org/10.1109/CVPR.2017.19
12. Liu, S.; Song, Y.; Cai, W.; Pujol, S.; Kikinis, R.; Wang, X.; Feng, D.: Multifold Bayesian kernelization in Alzheimer's diagnosis. In: Mori, K., Sakuma, I., Sato, Y., Barillot, C., Navab, N. (eds.) Medical Image Computing and Computer-Assisted Intervention—MICCAI 2013, pp. 303–310. Springer, Berlin, Heidelberg (2013)
13. Martin, R.C.; Gerstenecker, A.T.; Triebel, K.; Falola, M.I.; McPherson, T.; Cutter, G.R.; Marson, D.C.: Declining financial capacity in mild cognitive impairment: a six-year longitudinal study. Archiv. Clin. Neuropsychol. **34**, 152–161 (2019). https://doi.org/10.1093/arclin/acy030
14. Mirza, M.; Osindero, S.: Conditional generative adversarial nets. CoRR 1411, p. 1784 (2014). https://doi.org/10.48550/arXiv.1411.1784
15. Simonyan, K.; Zisserman, A.: Two-stream convolutional networks for action recognition in videos. CoRR 1406, p. 2199 (2014). https://doi.org/10.48550/arXiv.1406.2199
16. Zhang, D.; Wang, Y.: Multimodal classification of Alzheimer's disease and mild cognitive impairment. NeuroImage **55**, 856–867 (2011). https://doi.org/10.1016/j.neuroimage.2011.01.008
17. Zhang, J.; Liu, M.; An, L.; Gao, Y.; Shen, D.: Alzheimer's disease diagnosis using landmark-based features from longitudinal structural MR images. IEEE J. Biomed. Health Inform. **21**(6), 1607–1616 (2017). https://doi.org/10.1109/JBHI.2017.2704614
18. Sinharoy, R.; Sen, A.: Cardiovascular disease prediction using ensemble classification algorithm in machine learning **12**, 2628–2633 (2022). https://doi.org/10.21917/ijsc.2022.0366
19. Kazuhiro, K.: Generative adversarial networks for the creation of realistic artificial brain magnetic resonance images. Tomography **4**, 159–163 (2018). https://doi.org/10.18383/j.tom.2018.00042
20. King, R.D.; Brown, B.; Hwang, M.; Jeon, T.; George, A.T.: Fractal dimension analysis of the cortical ribbon in mild Alzheimer's disease. Neuroimage **53**, 471–479 (2010). https://doi.org/10.1016/j.neuroimage.2010.06.050
21. Kruger, A.: Implementation of a fast box-counting algorithm. Comput. Phys. Commun. **98**(1), 224–234 (1996). https://doi.org/10.1016/0010-4655(96)00080-X
22. Li, J.; Du, Q.; Sun, C.: An improved box-counting method for image fractal dimension estimation. Pattern Recognit. **42**, 2460–2469 (2009). https://doi.org/10.1016/j.patcog.2009.03.001
23. Liu, S.; Liu, S.; Cai, W.; Che, H.; Pujol, S.; Kikinis, R.; Feng, D.; Fulham, M.J.: ADNI: multimodal neuroimaging feature learning for multiclass diagnosis of Alzheimer's disease. IEEE Trans. Biomed. Eng. **62**(4), 1132–1140 (2015). https://doi.org/10.1109/TBME.2014.2372011
24. Yu, W.; Lei, B.; Wang, S.; Liu, Y.; Feng, Z.; Hu, Y.; Shen, Y.; Ng, M.K.: Morphological feature visualization of Alzheimer's disease via multidirectional perception GAN. IEEE Trans. Neural Netw. Learn. Syst. **2**, 1–15 (2022). https://doi.org/10.1109/TNNLS.2021.3118369
25. Li, X.; Du, Z.; Huang, Y.; Tan, Z.: A deep translation (GAN) based change detection network for optical and SAR remote sensing images. ISPRS J. Photogramm. Remote Sens. **179**, 14–34 (2021). https://doi.org/10.1016/j.isprsjprs.2021.07.007
26. Qu, C.; Zou, Y.; Ma, Y.; Chen, Q.; Luo, J.; Fan, H.; Jia, Z.; Gong, Q.; Chen, T.: Diagnostic performance of generative adversarial network-based deep learning methods for Alzheimer's disease: a systematic review and meta-analysis. Front. Aging Neurosci. **14**, 841696 (2022). https://doi.org/10.3389/fnagi.2022.841696
27. Zhou, X.; Qiu, S.; Joshi, P.S.; Xue, C.; Killiany, R.J.; Mian, A.Z.; Chin, S.P.; Au, R.; Kolachalama, V.B.: Enhancing magnetic resonance imaging-driven Alzheimer's disease classification performance using generative adversarial learning. Alzheimers Res. Ther. **13**(1), 60 (2021). https://doi.org/10.1186/s13195-021-00797-5
28. Sajjad, M.; Ramzan, F.; Khan, M.U.G.; Rehman, A.; Kolivand, M.; Fati, S.M.; Bahaj, S.A.: Deep convolutional generative adversarial network for Alzheimer's disease classification using positron emission tomography (PET) and synthetic data augmentation. Microsc. Res. Tech. **84**(12), 3023–3034 (2021). https://doi.org/10.1002/jemt.23861
29. Li, F.; Cheng, D.; Liu, M.: Alzheimer's disease classification based on combination of multi-model convolutional networks. In: 2017 IEEE International Conference on Imaging Systems and Techniques (IST), vol. 1, pp. 1–5 (2017). https://doi.org/10.1109/IST.2017.8261566
30. Hosseini-Asl, E.; Ghazal, M.; Mahmoud, A.; Aslantas, A.; Shalaby, A.M.; Casanova, M.F.; Barnes, G.N.; Gimel'farb, G.; Keynton, R.; El-Baz, A.: Alzheimer's disease diagnostics by a 3d deeply supervised adaptable convolutional network. Front. Biosci. (Landmark Ed.) **23**(3), 584–596 (2018). https://doi.org/10.2741/4606
31. Suk, H.-I.; Lee, S.-W.; Shen, D.; Initiative, T.A.D.N.: Latent feature representation with stacked auto-encoder for AD/MCI diagnosis. Brain Struct. Funct. **220**(2), 841–859 (2015). https://doi.org/10.1007/s00429-013-0687-3
32. Wang, H.; Shen, Y.; Wang, S.; Xiao, T.; Deng, L.; Wang, X.; Zhao, X.: Ensemble of 3d densely connected convolutional network for diagnosis of mild cognitive impairment and Alzheimer's disease. Neurocomputing **333**, 145–156 (2019). https://doi.org/10.1016/j.neucom.2018.12.018

33. Feng, W.; Halm-Lutterodt, N.V.; Tang, H.; Mecum, A.; Mesregah, M.K.; Ma, Y.; Li, H.; Zhang, F.; Wu, Z.; Yao, E.; Guo, X.: Automated MRI-based deep learning model for detection of Alzheimer's disease process. Int. J. Neural Syst. **30**(06), 2050032 (2020). https://doi.org/10.1142/S012906572050032X. **PMID: 32498641**
34. Hussain, E.; Hasan, M.; Hassan, S.Z.; Hassan Azmi, T.; Rahman, M.A.; Zavid Parvez, M.: Deep learning based binary classification for Alzheimer's disease detection using brain MRI images. In: 2020 15th IEEE Conference on Industrial Electronics and Applications (ICIEA), vol. 1, pp. 1115–1120 (2020). https://doi.org/10.1109/ICIEA48937.2020.9248213
35. Magnin, B.; Mesrob, L.; Kinkingnéhun, S.; Pélégrini-Issac, M.; Colliot, O.; Sarazin, M.; Dubois, B.; Lehéricy, S.; Benali, H.: Support vector machine-based classification of Alzheimer's disease from whole-brain anatomical MRI. Neuroradiology **51**(2), 73–83 (2009). https://doi.org/10.1007/s00234-008-0463-x
36. Ahmed, B.; Mizotin, O.; Benois-Pineau, M.: Alzheimer's disease diagnosis on structural MR images using circular harmonic functions descriptors on hippocampus and posterior cingulate cortex. Comput. Med. Imaging Graph. **44**, 13–25 (2015). https://doi.org/10.1016/j.compmedimag.2015.04.007
37. Khvostikov, A.; Aderghal, K.; Krylov, A.; Catheline, G.; Benois-Pineau, J.: 3D inception-based CNN with SMRI and MD-DTI data fusion for Alzheimer's disease diagnostics **3**, 102–113 (2018). https://doi.org/10.13140/RG.2.2.30737.28006
38. Korolev, S.; Safiullin, A.; Belyaev, M.; Dodonova, Y.: Residual and plain convolutional neural networks for 3D brain MRI classification. In: 2017 IEEE 14th International Symposium on Biomedical Imaging (ISBI 2017), vol. 1, pp. 835–838 (2017). https://doi.org/10.1109/ISBI.2017.7950647
39. Pan, Y.; Liu, M.; Lian, C.; Zhou, T.; Xia, Y.; Shen, D.: Synthesizing missing pet from MRI with cycle-consistent generative adversarial networks for Alzheimer's disease diagnosis. Med. Image Comput. Comput. Assist. Interv. **11072**, 455–463 (2018). https://doi.org/10.1007/978-3-030-00931-1_52
40. Logan, R.; Williams, B.G.; Ferreira da Silva, M.; Indani, A.; Schcolnicov, N.; Ganguly, A.; Miller, S.J.: Deep convolutional neural networks with ensemble learning and generative adversarial networks for Alzheimer's disease image data classification. Front. Aging Neurosci. **13**, 720226 (2021)